Article:
Pollock, A.M.T., Crowther, P.A., Bestenlehner, J.M. et al. (2025) Melnick 39 is a very massive intermediate-period colliding-wind binary. Monthly Notices of the Royal Astronomical Society, 539 (2). pp. 1291-1298. ISSN: 0035-8711

https://doi.org/10.1093/mnras/staf501

Monthly Notices of the ROYAL ASTRONOMICAL SOCIETY

MNRAS **539,** 1291–1298 (2025) https://doi.org/10.1093/mnras/staf501
Advance Access publication 2025 March 27

Melnick 39 is a very massive intermediate-period colliding-wind binary

A. M. T. Pollock [1]★ P. A. Crowther [1] J. M. Bestenlehner [1] Patrick S. Broos[2] and Leisa K. Townsley[2]†

[1]*Astrophysics Research Cluster, School of Mathematical and Physical Sciences, University of Sheffield, Hounsfield Road, Sheffield S3 7RH, UK*
[2]*Department of Astronomy & Astrophysics, 525 Davey Laboratory, Pennsylvania State University, University Park, PA 16802, USA*

Accepted 2025 March 20. Received 2025 March 20; in original form 2024 July 18

ABSTRACT

Individually identified binary systems of very massive stars define fixed points on possible evolutionary pathways that begin with extreme star formation and end in either coalescence of compact remnants or complete disruption as pair-production supernovae. The Large Magellanic Cloud star Melnick 39 in the Tarantula Nebula is revealed to be an eccentric ($e = 0.618 \pm 0.014$) binary system of a reasonably long period from time series analysis of *Chandra* T-ReX (The Tarantula – Resolved by X-rays) X-ray observations. Its X-ray luminosity scales with the inverse of the binary separation, as expected for colliding-wind binaries in the adiabatic regime. The inclusion of optical time series spectroscopy from the VLT-FLAMES Tarantula Survey and archival *Hubble Space Telescope* spectroscopy confirms Melnick 39 as a double-lined O2.5 If/WN6+O3 V–III spectroscopic binary with orbital period near 648 d. We obtain a mass ratio of $q = 0.76 \pm 0.06$, and minimum dynamical masses of 105 ± 11 and $80 \pm 11\,\mathrm{M}_\odot$ for the O2.5 If/WN6 and O3 V–III components, plus photometric evidence for an orbital inclination near 90°. Disentangled spectroscopy allows the physical and wind properties of the primary to be determined, including $T_* = 44$ kK, $\log L/\mathrm{L}_\odot = 6.2$, and $\log \dot{M}/\mathrm{M}_\odot\ \mathrm{yr}^{-1} = -5.0$. Its dynamical mass agrees closely with $109\,\mathrm{M}_\odot$ obtained from the mass–luminosity relation of very massive stars.

Key words: shock waves – binaries: spectroscopic – stars: massive – stars: winds, outflows – stars: Wolf–Rayet – X-rays: stars.

1 INTRODUCTION

The detection of compact mergers by LIGO (Laser Interferometer Gravitational Wave Observatory)/Virgo gravitational wave observatories has led to renewed interest in massive binaries, especially within the low-metallicity environments of the Magellanic Clouds, some of which may have been identified as candidate progenitors of black hole mergers (Belczynski et al. 2022). It is now established that the majority of massive stars are members of binary systems (Sana et al. 2012, 2013). Long-period systems can be identified via high spatial resolution imaging or interferometry, while short-period systems are preferentially detected through eclipses or spectroscopic campaigns (Moe & Di Stefano 2017).

X-ray monitoring offers one route to identifying the more observationally challenging intermediate-period systems owing to X-ray variability arising from wind–wind collisions within eccentric orbits. The Tarantula Nebula hosts the richest massive stellar population within the Local Group (Crowther 2019) and has been observed with the *Chandra* X-ray Visionary Project 'The Tarantula – Resolved by X-rays' designated T-ReX (Townsley, Broos & Povich 2024). Some of its X-ray light curves have indeed been used to identify candidate binary systems such as Melnick 34 (Pollock et al. 2018; Tehrani et al. 2019) and Melnick 33Na (Bestenlehner et al. 2022) subsequently confirmed as such.

Melnick 39[1] (Melnick 1985, hereafter Mk 39; also known as VFTS 482, Brey 78, or BAT99 99 notwithstanding some SIMBAD name confusion) is an Of/WN star (Walborn & Blades 1997; Crowther & Walborn 2011), located at a projected distance of 3 pc north-west of R136 at the heart of the Tarantula Nebula. Spectroscopic analysis of Mk 39 by Bestenlehner et al. (2014) revealed a very high bolometric luminosity ($\log L/\mathrm{L}_\odot \sim 6.4$) and inferred stellar mass ($\sim 145\,\mathrm{M}_\odot$). Mk 39 is one of the brightest X-ray sources in the Tarantula Nebula (Portegies Zwart, Pooley & Lewin 2002; Townsley et al. 2006). Crowther et al. (2022) analysed the cumulative T-ReX data set to determine a mean $\log L_\mathrm{X}/(\mathrm{erg\,s}^{-1}) = 34.3$, while other tentative evidence for binarity has also been reported (Massey, Penny & Vukovich 2002; Massey et al. 2005) including a preliminary orbital period of 92.6 ± 0.3 d from radial velocity variability (Schnurr et al. 2008). These collective characteristics are strongly suggestive of a colliding-wind binary system involving very massive components (Stevens, Blondin & Pollock 1992).

Large samples of OB stars in the Tarantula Nebula were observed spectroscopically via the VLT/FLAMES Tarantula Survey (VFTS; Evans et al. 2011), which included Mk 39, although follow-up radial velocity studies have been focused on normal OB stars (Mahy et al. 2020; Villaseñor et al. 2021). In this paper, we confirm the binary nature of Mk 39, establish its orbital period, and determine its component mass ratio from analysis of VFTS and archival *Hubble Space Telescope* (*HST*) spectroscopy.

★ E-mail: A.M.Pollock@sheffield.ac.uk
† Published posthumously.

[1]SIMBAD: 'Cl* NGC 2070 MEL 39'.

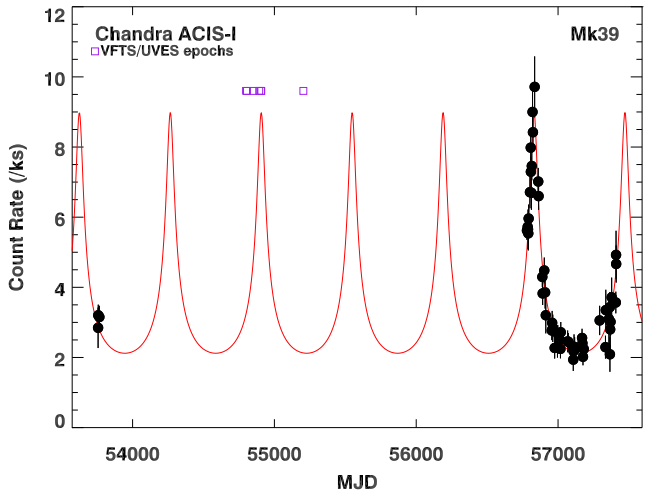

Figure 1. Least-squares fit of $1/D$ to *Chandra* ACIS-I T-ReX sensitivity-corrected count rates of Mk 39 supplemented by earlier ACIS-I data from 2006 (Townsley et al. 2014) implying $P = 641.1^{+4.3}_{-3.3}$ d, $e = 0.618 \pm 0.014$, and $T_0 = 56830.6 \pm 1.4$ MJD. Also shown are the seven epochs, some overlapping, of the VFTS optical spectroscopy reported in Table 2.

2 ORBITAL PERIOD OF MK 39 FROM X-RAYS

The 2 Ms *Chandra* T-ReX program (Townsley et al. 2024) was obtained over 630 d between 2014 May 3 and 2016 January 22 using the Advanced CCD Imaging Spectrometer – I (ACIS-I) instrument centred on R136a, the central cluster of the Tarantula Nebula. For this study, we incorporate 92 ks of ACIS observations from 2006 January 21–30 (Townsley et al. 2014). Data reduction, point-source detection, and extraction are summarized in Crowther et al. (2022) who noted that Mk 39 is an X-ray variable. The X-ray luminosities of colliding-wind binaries in the adiabatic regime are expected to depend on the inverse of the binary separation, D, (e.g. Stevens et al. 1992) as observed closely to apply over most of the long-period eccentric orbit of WR 140 (Pollock et al. 2021). Fig. 1 provides a least-squares fit of $1/D$ to the full data set, revealing an excellent match for an orbital period of $P = 641.1^{+4.3}_{-3.3}$ d, $e = 0.618 \pm 0.014$, and $T_0 = 56830.6 \pm 1.4$ MJD. The inferred orbital period narrowly exceeds the length of the 2014–2016 T-ReX campaign, which provides a strict lower limit to the period as the rising portion of the light curve at the end of the T-ReX campaign did not reach the level observed at the beginning. This also accounts for asymmetric errors in the period estimate. Critical in obtaining the solution were individual observation sensitivity corrections and the inclusion of the measurements made in 2006. Details of the X-ray solution and an observation log are given in Appendix A. Table 1 shows the final set of Keplerian orbital parameters derived below using constraints provided by the X-ray measurements.

3 OPTICAL ORBITAL SOLUTION FOR MK 39

In order to assess the reliability of the X-ray orbital solution of Mk 39 (VFTS 482) and establish the nature of the individual components, we have taken advantage of archival spectroscopy acquired at seven epochs via the VFTS (Evans et al. 2011) between 2008 December 3 and 2010 January 8 (MJD 54803–55204) with the Ultraviolet–Visual Echelle Spectrograph (UVES; D'Odorico et al. 2000). For each epoch two exposures of 1815 s were obtained with the red arm using the λ520 nm central wavelength, providing coverage between 4175–5155 and 5240–6200 Å at a spectral resolution of $R = 53\,000$.

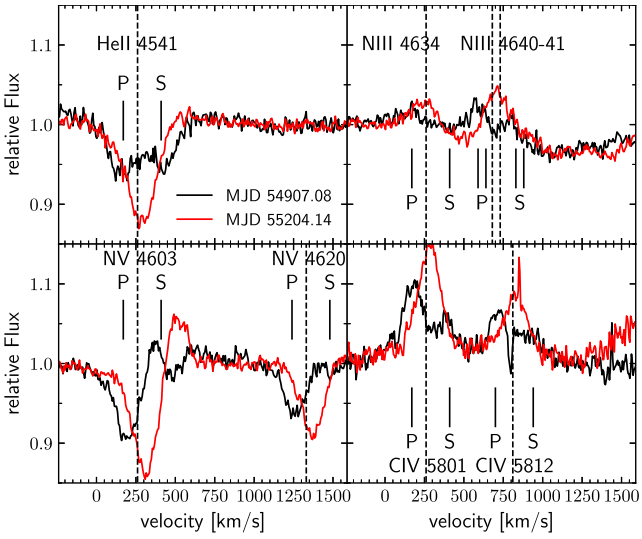

Figure 2. Observed VLT/UVES radial velocities of selected lines of Mk 39 at two contrasting epochs indicating systemic velocities with dotted lines and separate primary (P) and secondary (S) components when the lines are double.

Table 1. Keplerian orbital solution for Mk 39 from fits to the T-ReX X-ray light curve (Townsley et al. 2024) and to optical spectroscopy obtained in this study from VFTS (Evans et al. 2011) and *HST* (Massey et al. 2005).

Parameter	Result	Method
P	648.6 ± 0.9 d	VFTS, *HST*
T_0 (MJD)	56830.6 ± 1.4	*Chandra* T-ReX
e	0.618 ± 0.014	*Chandra* T-ReX
K_1	76.9 ± 4.3 km s^{-1}	VFTS, *HST*
K_2	101.4 ± 6.6 km s^{-1}	VFTS, *HST*
$v_{\rm sys}$	260.5 ± 3.2 km s^{-1}	VFTS, *HST*
ω	$130.4^\circ \pm 3.6^\circ$	VFTS, *HST*

UVES reveals spectroscopic variability of Mk 39, including double lines of He II λλ4542, 5412 from 2009 March 3–17 (MJD 54893–54907), as indicated in Fig. 2, fortuitously corresponding to what proves to be a quadrature phase near X-ray maximum (Fig. 1), supporting the X-ray orbital solution and establishing Mk 39 as a double-lined spectroscopic binary (SB2). He II λ4686 is severely blended at all epochs, while the cores of the H β and H γ absorption lines are contaminated with strong nebular emission.

We have supplemented Very Large Telescope (VLT)/UVES spectroscopy of Mk 39 with the archival *HST*/Faint Object Spectrograph (FOS) spectroscopy described by Massey et al. (2005) from 1997 January 1 (GO 6417, PI: P. Massey) and *HST*/Space Telescope Imaging Spectrograph (STIS) spectroscopy from 1998 February 4 (GO 7739, PI: P. Massey). The FOS data set used the G400H grating, covering λλ3235–4781 at $R \sim 1300$. The STIS data set used the G430M/4451 setting, covering λλ4310–4593 at $R \sim 6000$, while the G750M/6581 setting covers λλ6297–6866 at $R \sim 5000$ and includes H α. These data sets greatly extend the He II λ4542 spectroscopic baseline, and so help to constrain the orbital period of the system.

Mk 39 has received previous spectral classifications of O4 If (Melnick 1985), O3 If*/WN6 (Walborn & Blades 1997), O2 If* (Massey et al. 2005), and O2.5 If/WN6 (Crowther & Walborn 2011), the latter based on the UVES data used here. The primary is confirmed as an O2.5 If/WN6 star, since the morphology of H β is a clear P Cygni profile. The UVES observations close to periastron

Table 2. Radial velocities in km s^{-1} of spectral features in the primary and secondary components of Mk 39 from VLT/UVES spectroscopy. Epochs correspond to the mid-points of observations.

MJD	He II λ4542		N V λ4603	N III λ4641	He II λ5412		C IV λ5801
	Primary	Secondary	Primary	Primary	Primary	Secondary	Primary
54803.17	$290.9^{+3.0}_{-3.3}$	$210.1^{+3.2}_{-3.4}$	$299.2^{+3.9}_{-3.8}$	$248.7^{+5.1}_{-5.1}$	$305.0^{+3.9}_{-4.0}$	$188.3^{+3.8}_{-4.1}$	$291.7^{+4.6}_{-4.7}$
54803.22	$292.3^{+2.8}_{-2.8}$	$205.1^{+2.5}_{-3.8}$	$300.7^{+3.7}_{-3.7}$	$240.4^{+4.1}_{-4.2}$	$301.1^{+3.6}_{-3.6}$	$185.4^{+3.6}_{-3.6}$	$290.5^{+4.5}_{-4.5}$
54851.10	$295.1^{+2.2}_{-4.3}$	$215.9^{+4.4}_{-4.2}$	$283.3^{+3.5}_{-3.5}$	$238.3^{+5.3}_{-5.3}$	$314.5^{+3.6}_{-3.6}$	$182.8^{+4.0}_{-3.6}$	$282.5^{+4.7}_{-4.7}$
54893.04	$105.9^{+4.8}_{-4.1}$	$401.7^{+3.8}_{-3.8}$	$157.8^{+3.9}_{-3.9}$	$95.5^{+7.0}_{-7.0}$	$114.1^{+4.5}_{-4.2}$	$398.4^{+5.4}_{-5.1}$	$171.0^{+4.2}_{-4.2}$
54906.01	$152.6^{+3.4}_{-3.9}$	$379.6^{+7.4}_{-7.2}$	$186.1^{+4.8}_{-4.8}$	$133.8^{+9.0}_{-9.1}$	$113.4^{+5.7}_{-5.6}$	$378.3^{+5.8}_{-5.8}$	$187.2^{+5.6}_{-5.8}$
54907.08	$132.6^{+4.8}_{-4.7}$	$396.4^{+5.9}_{-4.2}$	$177.9^{+3.3}_{-3.3}$	$135.1^{+4.7}_{-4.7}$	$138.4^{+3.8}_{-3.7}$	$364.8^{+4.2}_{-4.2}$	$198.3^{+4.5}_{-4.5}$
55204.14	$294.2^{+3.2}_{-3.0}$	$215.7^{+3.8}_{-3.9}$	$297.1^{+3.7}_{-3.7}$	$253.9^{+4.1}_{-4.1}$	$298.5^{+3.2}_{-3.0}$	$195.3^{+3.8}_{-3.9}$	$293.2^{+4.4}_{-4.4}$

Table 3. Radial velocities in km s^{-1} of primary and secondary components of Mk 39 from cross-correlation of VLT/UVES and *HST*/FOS + STIS spectroscopy. Epochs correspond to the mid-points of observations.

MJD	Data set	Primary	Secondary
50449.89	*HST*/FOS	183 ± 10	336 ± 10
50848.83	*HST*/STIS	309 ± 10	205 ± 10
54803.17	VLT/UVES	315 ± 7	195 ± 7
54803.22	VLT/UVES	315 ± 7	196 ± 7
54851.10	VLT/UVES	303 ± 7	225 ± 7
54893.04	VLT/UVES	125 ± 6	393 ± 5
54906.01	VLT/UVES	140 ± 6	366 ± 5
54907.08	VLT/UVES	147 ± 5	361 ± 5
55204.14	VLT/UVES	288 ± 9	226 ± 8

Table 4. Physical properties of the primary and secondary components of Mk 39 from this study.

Property	Primary	Secondary	Reference
Spectral type	O2.5 If/WN6	O3 V–III	This study
$T_{\rm eff}$ (kK)	44 ± 2.5	48 ± 2.5	This study
$\log(L/{\rm L}_\odot)$	6.20 ± 0.15	6.00 ± 0.15	This study
$\log \dot{M}/{\rm M}_\odot\ {\rm yr}^{-1}$	–5.0 ± 0.2	$-6.2^{+0.2}_{-0.5}$	This study
v_∞ (km s^{-1})	2600	2600:	Bestenlehner et al. (2014)
Y	0.30 ± 0.05	0.27 ± 0.05	This study
$v_{\rm eq}\ \sin i$ (km s^{-1})	100	80	This study
$M_{\rm dyn} \sin i$ (M$_\odot$)	105.2	79.8	This study
M (M$_\odot$)	109 ± 7	83 ± 5	Gräfener et al. (2011)
$M_{\rm evol}$ (M$_\odot$)	83^{+20}_{-18}	69^{+14}_{-11}	BONNSAI
τ (Myr)	1.5 ± 0.3	$1.1^{+0.3}_{-0.8}$	BONNSAI

(Fig. 2) permit the spectral type of the secondary to be determined. From comparison with early-O templates (Walborn et al. 2002), He II λλ4542, 5412 are strong, with He I λ4471 weak or absent, plus weak N V λλ4603–4620 absorption and N III λλ4634–4641 emission, implying O3 V–III for the secondary.

We have undertaken single or double Gaussian fits to various optical absorption lines in VLT/UVES spectra to establish the individual component radial velocities presented in Table 2. In addition, we have used a grid of CMFGEN model atmospheres (Hillier & Miller 1998) suitable for early-type O stars of Large Magellanic Cloud (LMC) metallicity (Bestenlehner et al. 2014) to cross-correlate with VLT/UVES and *HST*/FOS + STIS spectroscopy. Radial velocities of the primary and secondary components are presented in Table 3, having been derived by investigating the extrema and zero-points of the second and third derivatives of the cross-correlation function.

To derive the orbital parameters we have used these uncertainty-weighted averages and employed the Markov chain Monte Carlo approach of Tehrani et al. (2019). As the VLT/UVES data provide poor orbital phase coverage, we fixed the eccentricity to the X-ray photometric solution from Section 2 and utilized $T_0 = 56830.6 \pm 1.4$ MJD as a prior. We obtained the solution reported in Table 1 and illustrated in Fig. 3 with period $P = 648.6 \pm 0.9$ d, leading to minimum masses $M_1 \sin^3 i = 105 \pm 11\ {\rm M}_\odot$ and $M_2 \sin^3 i = 80 \pm 11\ {\rm M}_\odot$ and mass ratio $q = K_1/K_2 = M_2/M_1 = 0.76 \pm 0.06$. The systemic velocity $v_{\rm sys} = 260 \pm 3$ km s^{-1} of Mk 39 is close to the mean radial velocity of 268 ± 6 km s^{-1} of OB stars within 5 pc of R136 (Hénault-Brunet et al. 2012).

The X-ray and optical period estimates differ by between 1σ and 2σ due to larger positive errors in the X-ray value with any inconsistency probably reflecting systematic errors of which no account has been taken. Appendix A below discusses some of these in the X-ray 1/D regime. In the optical, the solution is quite well constrained by the appearance of double lines in three epochs over an interval of 14 d with the closest of the four epochs in which the double lines were not resolved in a key observation 42 d earlier. An alternative solution to that reported in Table 1 is available by exchanging primary and secondary radial velocities in that key observation at MJD 54851.10. Although this is formally superior in statistical terms, the implied period of $P = 653.2 \pm 0.4$ d is less consistent with the X-ray value. These uncertainties should be eliminated by future suitably well-timed observations in either X-ray photometry or optical spectroscopy around periastron the next of which is expected to occur in late 2026.

4 PHYSICAL AND WIND PROPERTIES OF MK 39

Armed with the orbital solution of Mk 39 from the previous section, we have disentangled the components of the UVES spectroscopy following the approach of Bestenlehner et al. (2022) for the SB2 system Mk 33Na, which includes rescaling according to the flux ratio of the individual components. For the physical and wind properties of the individual components of Mk 39, Bestenlehner et al. (2014) obtained a system luminosity of $\log L/{\rm L}_\odot = 6.4$ that we adopt here ($E(B-V) = 0.45$, $R_V = 3.26$), together with the mass ratio $q = 0.76$. For LMC very massive main-sequence stars $L \propto M^{1.4\pm0.2}$ (Köhler et al. 2015), so $L_2/L_1 \sim 0.7$ and $\log(L_1/{\rm L}_\odot) = 6.2$ and $\log(L_2/{\rm L}_\odot) = 6.0$.

Comparisons between disentangled UVES spectra (blue) and synthetic CMFGEN spectra (red) for each component are presented in Fig. 4 with the STIS H α region in Fig. 5. Disentangled secondary spectra at H γ and He II λ4686 are unreliable owing to the dominant

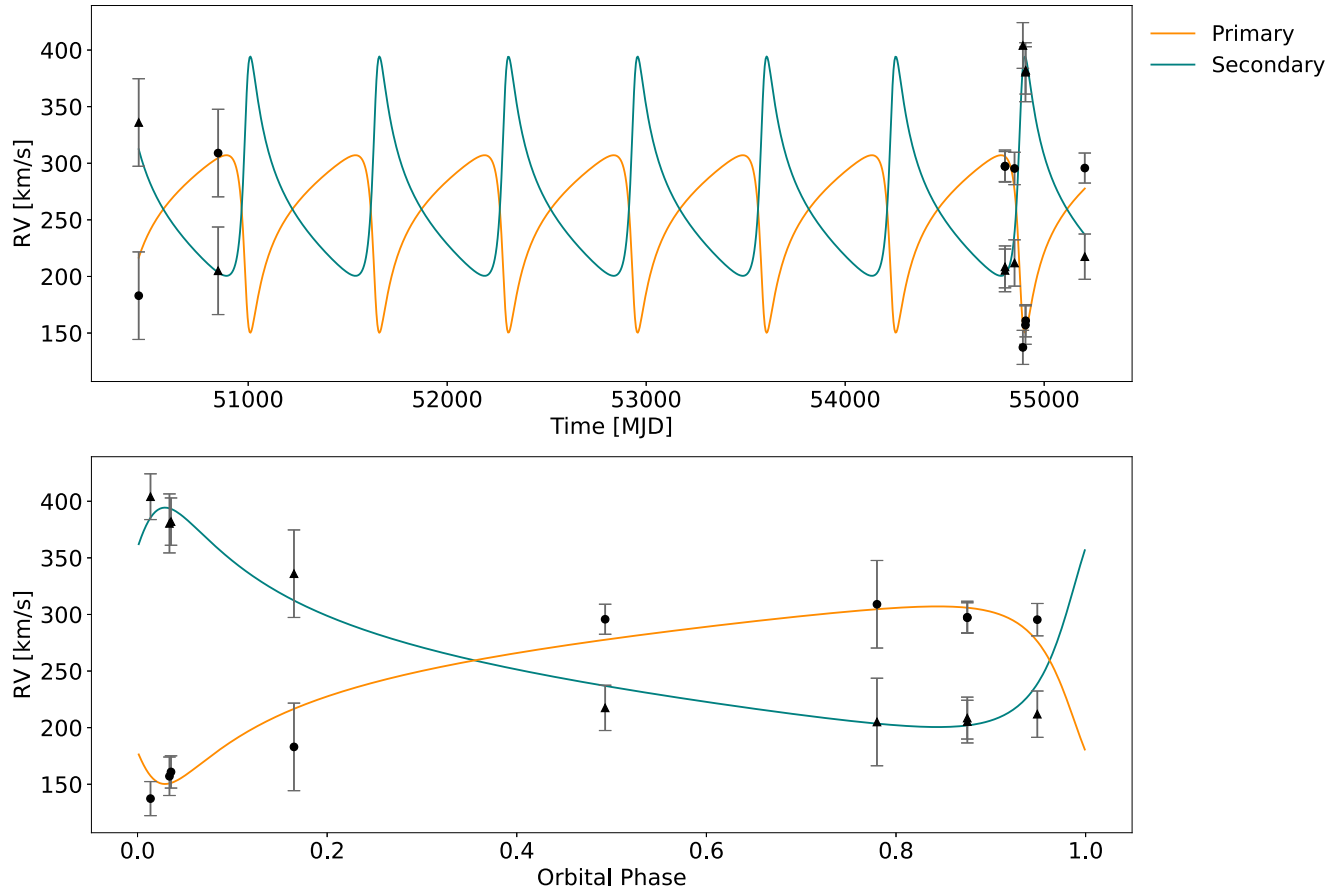

Figure 3. Orbital solution to He II λ4542 VLT (UVES) and *HST* (FOS + STIS) radial velocities for the primary (filled circles) and secondary (filled triangles) components of Mk 39, revealing $K_1 = 76.9$ km s^{-1} and $K_2 = 101.4$ km s^{-1}, $v_{\rm sys} = 260 \pm 3$ km s^{-1}, $P = 648.6 \pm 0.9$ d for $e = 0.618$ obtained from X-ray light-curve fit, implying a mass ratio of $q = 0.76 \pm 0.06$.

primary spectral lines as well as nebular Balmer line contamination. We obtain stellar temperatures of $T_* = 44.0 \pm 2.5$ and 48.0 ± 2.5 kK, respectively, for the primary and secondary from N V λλ4603–4620 and He II λ4542/λ5411 since He I λλ4471, 5876 are dominated by nebular emission. N IV λ4058 is not included in the UVES data, so the use of solely nitrogen diagnostics would rely on the N V doublet and N III λλ4634–4641, requiring a lower temperature for the primary and higher temperature for the secondary, subject to uncertainties in their nitrogen abundances. Weak emission in the C IV λλ5801–5812 doublet is seen in both components and is reasonably well reproduced for our preferred stellar temperatures.

We favour a mass-loss rate of about 10^{-5} M$_\odot$ yr^{-1} for the primary from He II λ4686, supported by the morphology of H β and the STIS H α spectroscopy, whereas $10^{-6.2}$ M$_\odot$ yr^{-1} is estimated for the secondary owing to an absence of any suitable wind diagnostics. A wind velocity of 2600 km s^{-1} is adopted for both components following Bestenlehner et al. (2014) who analysed archival far-ultraviolet (UV) STIS/G140L spectroscopy of Mk 39 from Massey et al. (2005). We estimate equatorial rotational velocities $v_{\rm eq} \sin i \sim$ 100 and 80 km s^{-1} from He II λλ4542, 5412 lines.

High-resolution far-UV spectroscopy of Mk 39 has been obtained via the *HST* ULLYSES (Ultraviolet Legacy Library of Young Stars as Essential Standards) survey of massive stars in the Magellanic Clouds (Roman-Duval et al. 2020), using Cosmic Origins Spectrograph (COS) G130M/1291 and G160M/1611, providing spectral coverage in the range λλ1131–1790 at a spectral resolution of $R \sim 15\,000$. These data sets were not used for our analysis, but the synthetic spectra provide a good match to O V λ1371, Si IV λλ1393–1402, He II λ1640, and N IV λ1718, while P Cygni emission for C IV λλ1548–1551 and N V λλ1238–1242 is underestimated, the latter mitigated by strong Lyα interstellar absorption and its sensitivity to X-ray production (excluded from our spectroscopic analysis). The reddened spectral energy distribution of Mk 39 provides a good match to COS far-UV, plus more recent STIS near-UV (G230LB) and blue visual (G430L) spectroscopy (GO 16230, PI: D Massa).

The BONN Stellar Astrophysics Interface (BONNSAI;[2] Schneider et al. 2014) coupled to evolutionary models from Köhler et al. (2015) and empirical initial rotation velocities of Ramírez-Agudelo et al. (2013) infer stellar masses and ages of $M_{\rm evol} = 83^{+20}_{-18}$ and 69^{+14}_{-11} M$_\odot$ and 1.5 ± 0.3 and $1.1^{+0.3}_{-0.8}$ Myr for the primary and secondary, assuming the stars have evolved independently to date. These evolutionary mass estimates are somewhat lower than minimum dynamical mass determinations (BONNSAI underpredicts stellar luminosities by 0.1 dex). The favoured age is consequently ∼1.4 Myr, similar to the nearby massive star cluster R136 (Crowther et al. 2016; Brands et al. 2022). Alternatively, $M \sim 109 \pm 7$ and 83 ± 5 M$_\odot$ are obtained for the primary and secondary from the mass–luminosity

[2]The BONNSAI web service is available at www.astro.uni-bonn.de/stars/bonnsai.

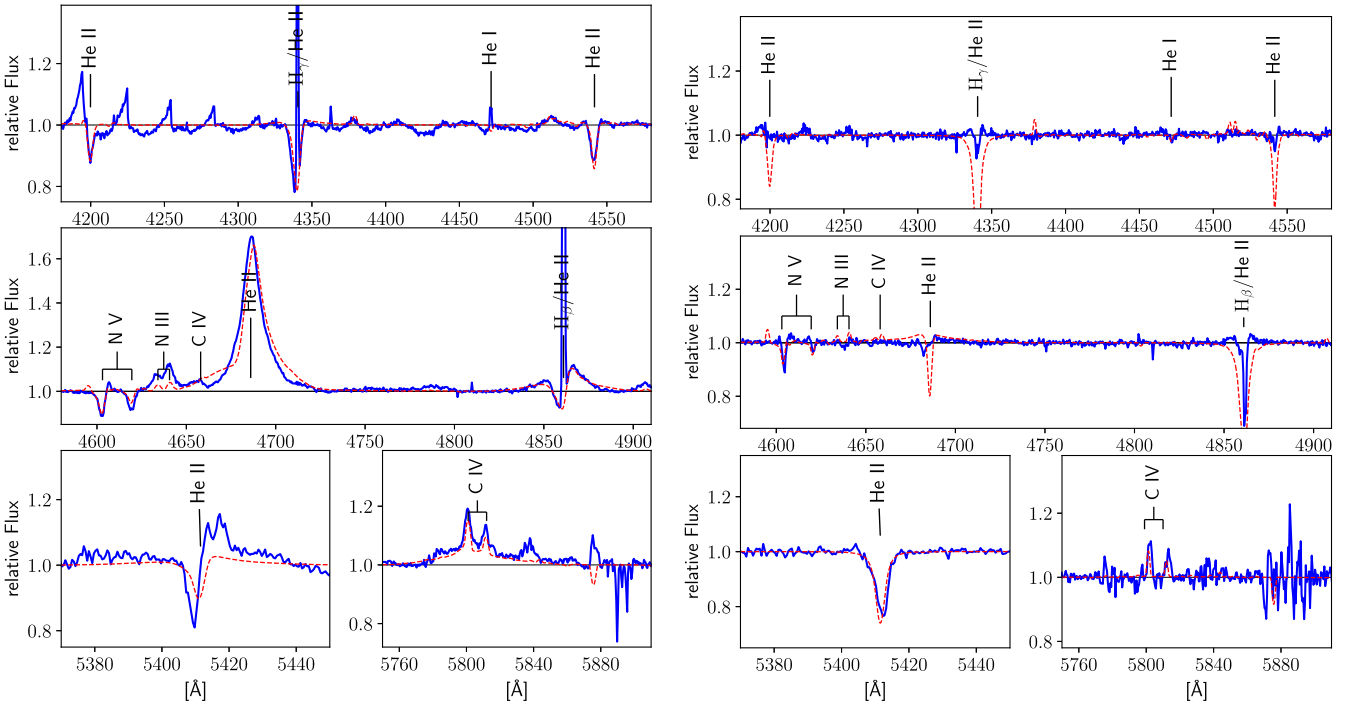

Figure 4. Comparison between disentangled Mk 39 primary (left) and secondary (right) UVES spectroscopy (solid blue lines) and synthetic CMFGEN spectra (dotted red lines). Strong nebular lines (Balmer, He I, and [O III]) are present in the left panel, together with instrumental emission features shortward of λ4300.

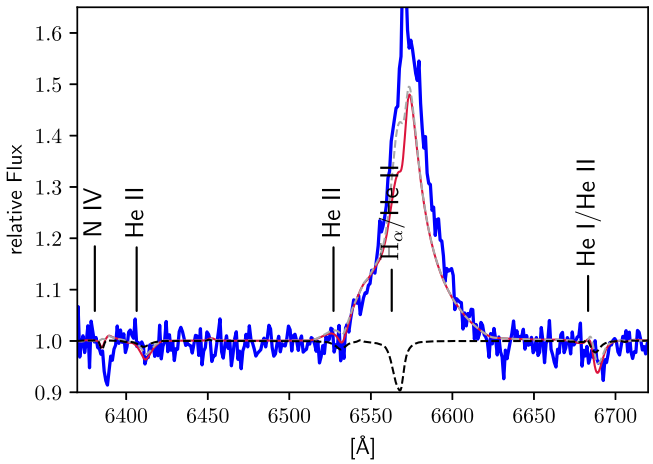

Figure 5. *HST*/STIS spectroscopy of Mk 39 near Hα (solid blue) arising from a combination of dominant primary emission and weak secondary absorption.

relationship for very massive stars (Gräfener et al. 2011), suggesting an inclination close to $i = 90°$.

Massey et al. (2002, their fig. 5) reported a short-lived ∼0.1 mag photometric dip in the optical light curve of Mk 39 (alias HSH 7; Hunter et al. 1995) at MJD 51635.36-51. Our preferred orbital solution in Table 1 would suggest a conjunction with the primary in front at MJD 51627.5 ± 7.5 with most of the uncertainty due to the orbital timing of period and periastron passage rather than the orbital geometry of eccentricity and longitude of periastron. Thus a period shorter within the error budget by 1.0 d would bring consistency between the orbital solution and the occurrence of a photometric dip due to a physical or wind eclipse that is clearly subject to confirmation to reinforce the suggestion of a high orbital inclination. The collected physical properties of the primary and secondary components of Mk 39 are shown in Table 4.

5 DISCUSSION AND CONCLUSIONS

We have established that the X-ray luminous Of/WN star Mk 39 in the Tarantula Nebula is an SB2 colliding-wind binary with a period of 648.6 ± 0.9 d that follows the inverse separation law for adiabatic emission. In this respect, Mk 39 represents an ideal example with little or none of the deviations from adiabatic behaviour seen in other systems near periastron due, for example, to competitive cooling seen in WR 140 (Pollock et al. 2021), circumstellar absorption in WR 25, another very massive binary system (Pradhan et al. 2021), or perhaps a combination of both in Mk 34 and WR 21a (Pollock et al. 2018).

Mk 39, which reaches a maximum count rate near 10 counts ks^{-1} at the minimum periastron orbital separation of 3.5 au according to the new orbital solution, may be compared with Mk 34, the brightest T-ReX colliding-wind binary at its minimum near 35 counts ks^{-1} (Pollock et al. 2018) at the similar but slightly larger separation maximum of 4.1 au reached at apastron (Tehrani et al. 2019). This difference is roughly consistent with expectations of scaling laws (Luo, McCray & Mac Low 1990; Stevens et al. 1992) which may be recast from mass-loss rate and terminal velocity to use luminosity and velocity full width at half-maximum, Δv, of the He II λ4686 wind line (Crowther, Rate & Bestenlehner 2023) to suggest $L_X \propto (L\Delta v^{-3.2})_{\rm He\,II}$: X-rays from the weaker, faster wind of Mk 39 fall a factor of a few short of the stronger, slower wind of Mk 34.

Optical spectroscopy has been used to determine a mass ratio of $q = 0.76 \pm 0.06$, and minimum component masses of $105 \pm 11\,M_\odot$

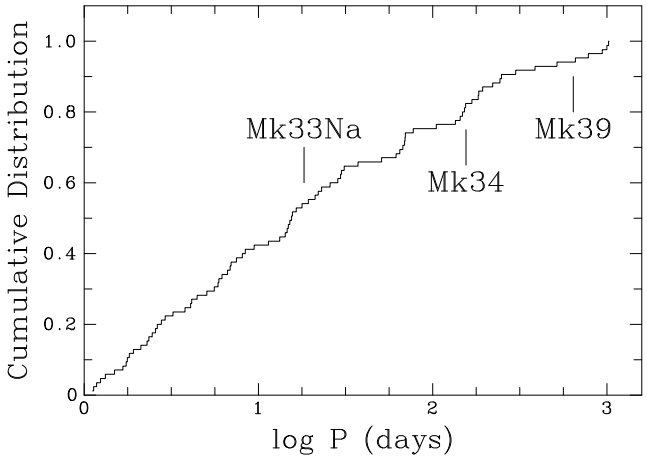

Figure 6. Cumulative distribution of orbital periods of OB stars in the Tarantula Nebula from Almeida et al. (2017) supplemented with T-ReX SB2 systems, Mk 34 (Tehrani et al. 2019), Mk 33Na (Bestenlehner et al. 2022), and Mk 39 from this study with some of the longest period binaries subject to revision.

(O2.5 If/WN6) and $80 \pm 11\,M_{\odot}$ (O3 V–III). These agree closely with the masses from the Gräfener et al. (2011) mass–luminosity relation for very massive stars based on physical properties determined from disentangled UVES spectroscopy, for an inclination close to 90°. The inability of Massey et al. (2005) to obtain a satisfactory spectroscopic fit for Mk 39 was attributed to its composite nature though Bestenlehner et al. (2014) obtained physical and wind properties of Mk 39 from VLT/UVES spectroscopy (Evans et al. 2011), supplemented by *HST*/STIS G140L and Hα spectroscopy (Massey et al. 2005) plus *K*-band VLT/SINFONI (Spectrograph for INtegral Field Observation in the Near-Infrared) spectroscopy.

The only previously published orbital solution was from Schnurr et al. (2008) who obtained $P = 92.6 \pm 0.3$ d, $K_1 = 91 \pm 19$ km s^{-1}, and $v_{\rm sys} = 337 \pm 16$ km s^{-1} from spectroscopic observations of He II λ4686, *assuming* – with explicit caution – a circular orbit. Although narrower photospheric absorption lines, such as He II λ4542 used in this study, are more straightforward diagnostics of Keplerian orbital motion than broader, slightly irregular, wind emission lines such as He II λ4686 used by Schnurr et al. (2008), the radial velocities of this emission line in the current VLT/UVES data follow reasonably closely the primary's absorption lines at roughly the same positive displacement of about 80 km s^{-1}. The inconsistency with the new orbital solution must lie elsewhere. According to the new ephemeris, it is plausible that the minimum and maximum radial velocity excursions that drive the earlier orbital solution coincide with quadratures near a projected periastron passage of the new eccentric solution on 2002 January 16 during the first season of observations, with the second season encompassing the subsequent apastron. However, this possibility fails because the maximum and minimum obtained during successive runs 20 d apart in 2001 December are too close together in time and too far apart in velocity to be consistent with the parameters in Table 1.

Bestenlehner et al. (2022, their table 5) provide a summary of massive binaries in the LMC. Of these, the most extreme systems are exclusive to the Tarantula Nebula: Mk 34 (WN5h+WN5h; Tehrani et al. 2019), R144 (WN5–6h + WN6–7h; Shenar et al. 2021), R139 (O6.5 Iafc + O6 Iaf; Mahy et al. 2020), and Mk 33Na (OC2.5 If+O4 V; Bestenlehner et al. 2022) with eccentric orbits in the range 18–155 d, and primary masses comfortably exceeding the previous LMC record holder (Massey et al. 2002).

Mk 39 has similar stellar components, albeit with a significantly longer period orbit, as indicated in Fig. 6 that shows a cumulative distribution of OB orbital periods for the Tarantula Nebula from Almeida et al. (2017), supplemented by T-ReX results. X-ray photometric surveys can help facilitate an improved characterization of orbital periods, eccentricities, and mass ratios of massive stars in the LMC, together with continuing spectroscopic surveys (Mahy et al. 2020; Villaseñor et al. 2021) at longer wavelengths.

ACKNOWLEDGEMENTS

This is part of a collection of papers publishing posthumously the unfinished work of LKT, the principal investigator of T-ReX. This work was supported by the *Chandra X-ray Observatory* General Observer grants GO5-6080X (PI: L. Townsley) and GO4-15131X (PI: L. Townsley) and by the Penn State ACIS Instrument Team Contract SV4-74108. All of these were issued by the *Chandra* X-ray Center, which is operated by the Smithsonian Astrophysical Observatory for and on behalf of NASA under contract NAS8-03060. Based in part on observations obtained with the NASA/ESA *Hubble Space Telescope*, retrieved from the *Mikulski Archive for Space Telescopes* (*MAST*) at the STScI. STScI is operated by the Association of Universities for Research in Astronomy, Inc. under NASA contract NAS 5-26555. PAC and JMB were supported by the Science and Technology Facilities Council research grant ST/V000853/1 (PI. V. Dhillon).

DATA AVAILABILITY

All the observational data used in this article are freely available as follows: the X-ray data through the *Chandra* Data Archive at https://cxc.cfa.harvard.edu/cda/; the optical VLT/FLAMES spectra through the ESO Archive Science Portal at https://archive.eso.org/scienceportal/home; and the optical *HST* data through the *Mikulski Archive for Space Telescopes* at https://mast.stsci.edu/portal/Mashup/Clients/Mast/Portal.html. The synthetic CMFGEN model atmospheres of the primary and secondary stars are available on request.

REFERENCES

Almeida L. A. et al., 2017, A&A, 598, A84
Belczynski K. et al., 2022, ApJ, 925, 69
Bestenlehner J. M. et al., 2014, A&A, 570, A38
Bestenlehner J. M., Crowther P. A., Broos P. S., Pollock A. M. T., Townsley L. K., 2022, MNRAS, 510, 6133
Brands S. A. et al., 2022, A&A, 663, A36
Crowther P. A., 2019, Galaxies, 7, 88
Crowther P. A., Walborn N. R., 2011, MNRAS, 416, 1311
Crowther P. A. et al., 2016, MNRAS, 458, 624
Crowther P. A., Broos P. S., Townsley L. K., Pollock A. M. T., Tehrani K. A., Gagné M., 2022, MNRAS, 515, 4130
Crowther P. A., Rate G., Bestenlehner J. M., 2023, MNRAS, 521, 585
D'Odorico S., Cristiani S., Dekker H., Hill V., Kaufer A., Kim T., Primas F., 2000, in Bergeron J., ed., Proc. SPIE Conf. Vol. 4005, Discoveries and Research Prospects from 8- to 10-Meter-Class Telescopes. SPIE, Bellingham, p. 121
Evans C. J. et al., 2011, A&A, 530, A108
Gräfener G., Vink J. S., de Koter A., Langer N., 2011, A&A, 535, A56
Hénault-Brunet V. et al., 2012, A&A, 546, A73
Hillier D. J., Miller D. L., 1998, ApJ, 496, 407
Hunter D. A., Shaya E. J., Holtzman J. A., Light R. M., O'Neil E. J., Jr, Lynds R., 1995, ApJ, 448, 179

Köhler K. et al., 2015, A&A, 573, A71
Luo D., McCray R., Mac Low M.-M., 1990, ApJ, 362, 267
Mahy L. et al., 2020, A&A, 634, A118
Massey P., Penny L. R., Vukovich J., 2002, ApJ, 565, 982
Massey P., Puls J., Pauldrach A. W. A., Bresolin F., Kudritzki R. P., Simon T., 2005, ApJ, 627, 477
Melnick J., 1985, A&A, 153, 235
Moe M., Di Stefano R., 2017, ApJS, 230, 15
Pollock A. M. T., Crowther P. A., Tehrani K., Broos P. S., Townsley L. K., 2018, MNRAS, 474, 3228
Pollock A. M. T. et al., 2021, ApJ, 923, 191
Portegies Zwart S. F., Pooley D., Lewin W. H. G., 2002, ApJ, 574, 762
Pradhan P., Huenemoerder D. P., Ignace R., Pollock A. M. T., Nichols J. S., 2021, ApJ, 915, 114
Ramírez-Agudelo O. H. et al., 2013, A&A, 560, A29
Roman-Duval J. et al., 2020, Res. Notes Am. Astron. Soc., 4, 205
Sana H. et al., 2012, Science, 337, 444
Sana H. et al., 2013, A&A, 550, A107
Schneider F. R. N., Langer N., de Koter A., Brott I., Izzard R. G., Lau H. H. B., 2014, A&A, 570, A66
Schnurr O., Moffat A. F. J., St-Louis N., Morrell N. I., Guerrero M. A., 2008, MNRAS, 389, 806
Shenar T. et al., 2021, A&A, 650, A147
Stevens I. R., Blondin J. M., Pollock A. M. T., 1992, ApJ, 386, 265
Tehrani K. A., Crowther P. A., Bestenlehner J. M., Littlefair S. P., Pollock A. M. T., Parker R. J., Schnurr O., 2019, MNRAS, 484, 2692
Townsley L. K., Broos P. S., Feigelson E. D., Garmire G. P., Getman K. V., 2006, AJ, 131, 2164
Townsley L. K., Broos P. S., Garmire G. P., Bouwman J., Povich M. S., Feigelson E. D., Getman K. V., Kuhn M. A., 2014, ApJS, 213, 1
Townsley L. K., Broos P. S., Povich M. S., 2024, ApJS, 273, 5
Villaseñor J. I. et al., 2021, MNRAS, 507, 5348
Walborn N. R., Blades J. C., 1997, ApJS, 112, 457
Walborn N. R. et al., 2002, AJ, 123, 2754

APPENDIX A: THE X-RAY ORBITAL SOLUTION

Fig. A1 shows the folded X-ray light curve resulting from the $1/D$ model of the observed T-ReX count rates logged in Table A1. Shown in grey are the observed count rate values scaled by the inverse ratio of the implied binary separation to the maximum separation at apastron, D_{1+e}. In a successful model, this quantity would be independent of phase. In this case, the observed dynamic range of about a factor of 5 is reproduced to within a few per cent both before periastron and in the less well-sampled data after. Defects appear to be largely absent which could have been due to a variety of potential instrumental or physical causes such as uncertainties in the often substantial count-rate corrections shown in the table or the effects of absorption through stellar winds close to conjunctions.

For the purposes of predicting the timing of future observations at or near periastron, in addition to the most accurately determined period of $P = 648.6 \pm 0.9$ d from the radial velocity analysis, it would be worth keeping in mind $P = 648.3 \pm 0.9$ d from the weighted mean of optical and X-ray values and $P = 647.6 \pm 1.4$ d from alignment of the putative photometric eclipse discussed in Section 4.

Table A1. Binary-phase-ordered log of *Chandra* observations in the T-ReX survey of 30 Doradus and three earlier observations with observation ID and epoch; exposure time, T; sensitivity factor relative to the ObsID 7264 maximum; sensitivity-corrected count rate per 1000 s of Mk 39; and phase interval covered, ϕ, of the 641.1-d best-fitting X-ray orbit centred on MJD 56830.6.

ObsID	Date	MJD	T (s)	Factor	Mk 39 (counts ks^{-1})	$\phi_{641.1}$(d)
16445	2015-05-27T00:18:12	57169.013	49 310	0.940	2.6 ± 0.3	-302.4 ± 0.3
17660	2015-05-29T14:55:28	57171.622	38 956	0.941	2.4 ± 0.3	-299.9 ± 0.2
16446	2015-06-02T11:50:14	57175.493	47 547	0.940	2.0 ± 0.2	-295.9 ± 0.3
17642	2015-06-08T05:11:14	57181.216	34 438	0.915	2.2 ± 0.3	-290.3 ± 0.2
16449	2015-09-28T05:35:14	57293.233	24 628	0.929	3.1 ± 0.4	-178.3 ± 0.2
18672	2015-11-08T01:04:22	57334.045	30 574	0.928	2.3 ± 0.3	-137.5 ± 0.2
18706	2015-11-10T17:09:59	57336.715	14 776	0.925	3.3 ± 0.6	-134.9 ± 0.1
18720	2015-12-02T10:49:02	57358.451	9832	0.928	3.1 ± 0.7	-113.2 ± 0.1
18721	2015-12-08T17:13:14	57364.718	25 598	0.926	3.4 ± 0.4	-106.8 ± 0.2
17603	2015-12-09T15:27:36	57365.644	13 778	0.929	2.1 ± 0.5	-106.0 ± 0.1
18722	2015-12-11T09:09:39	57367.382	9826	0.929	2.8 ± 0.7	-104.3 ± 0.1
18671	2015-12-13T23:41:12	57369.987	25 617	0.927	3.0 ± 0.4	-101.6 ± 0.2
18729	2015-12-21T22:10:30	57377.924	16 742	0.929	3.7 ± 0.6	-93.7 ± 0.1
18750	2016-01-20T00:41:30	57407.029	48 318	0.926	3.6 ± 0.3	-64.4 ± 0.3
18670	2016-01-21T20:59:37	57408.875	14 565	0.928	4.9 ± 0.7	-62.8 ± 0.1
18749	2016-01-22T16:14:19	57409.677	22 153	0.926	4.7 ± 0.5	-61.9 ± 0.1
16192	2014-05-03T04:10:27	56780.174	93 761	0.932	5.6 ± 0.3	-49.9 ± 0.6
16193	2014-05-08T10:15:25	56785.427	75 994	0.929	5.7 ± 0.3	-44.7 ± 0.5
16612	2014-05-11T02:15:31	56788.094	22 672	0.955	5.7 ± 0.6	-42.3 ± 0.2
16194	2014-05-12T20:00:24	56789.834	31 333	0.898	5.5 ± 0.5	-40.6 ± 0.2
16615	2014-05-15T08:24:45	56792.351	45 170	0.954	6.0 ± 0.4	-38.0 ± 0.3
16195	2014-05-24T14:09:28	56801.590	44 405	0.827	6.7 ± 0.5	-28.7 ± 0.3
16196	2014-05-30T00:05:56	56807.004	67 109	0.924	8.0 ± 0.4	-23.2 ± 0.4
16617	2014-05-31T01:27:04	56808.060	58 860	0.749	7.3 ± 0.4	-22.2 ± 0.4
16616	2014-06-03T22:26:17	56811.935	34 530	0.953	6.7 ± 0.5	-18.4 ± 0.2
16197	2014-06-06T12:32:26	56814.523	67 790	0.735	7.5 ± 0.4	-15.7 ± 0.4
16198	2014-06-11T20:20:49	56819.848	39 465	0.688	9.0 ± 0.6	-10.5 ± 0.2
16621	2014-06-14T14:46:41	56822.616	44 400	0.758	8.4 ± 0.5	-7.7 ± 0.3
16200	2014-06-26T20:01:47	56834.835	27 361	0.557	9.7 ± 0.9	$+4.4 \pm 0.2$

Table A1 – *continued*

ObsID	Date	MJD	T (s)	Factor	Mk 39 (counts ks^{-1})	$\phi_{641.1}$(d)
16201	2014-07-21T22:13:45	56859.926	58 390	0.894	7.0 ± 0.4	$+29.7 \pm 0.4$
16640	2014-07-24T11:21:26	56862.473	61 679	0.789	6.6 ± 0.4	$+32.3 \pm 0.4$
16202	2014-08-19T15:30:01	56888.646	65 128	0.935	4.3 ± 0.3	$+58.5 \pm 0.4$
17312	2014-08-22T06:21:18	56891.265	44 895	0.939	3.8 ± 0.3	$+61.0 \pm 0.3$
16203	2014-09-02T12:47:11	56902.533	41 423	0.946	4.5 ± 0.4	$+72.2 \pm 0.3$
17413	2014-09-08T15:21:28	56908.640	24 650	0.931	3.9 ± 0.5	$+78.2 \pm 0.2$
17414	2014-09-13T12:24:59	56913.517	17 317	0.942	3.2 ± 0.5	$+83.0 \pm 0.1$
16442	2014-10-25T13:38:44	56955.569	48 350	0.943	2.8 ± 0.3	$+125.3 \pm 0.3$
17545	2014-10-28T04:14:57	56958.177	34 530	0.941	3.0 ± 0.3	$+127.8 \pm 0.2$
5906	2006-01-21T19:04:02	53756.794	12 317	0.997	2.8 ± 0.6	$+132.0 \pm 0.1$
17544	2014-11-01T16:52:08	56962.703	25 642	0.942	2.8 ± 0.4	$+132.3 \pm 0.2$
7263	2006-01-22T16:51:51	53757.703	42 528	0.997	3.2 ± 0.3	$+133.1 \pm 0.3$
7264	2006-01-30T15:06:27	53765.629	37 593	1.000	3.2 ± 0.3	$+141.0 \pm 0.2$
16443	2014-11-14T23:14:31	56975.968	34 530	0.944	2.3 ± 0.3	$+145.6 \pm 0.2$
17486	2014-12-04T13:39:50	56995.569	33 541	0.941	2.3 ± 0.3	$+165.2 \pm 0.2$
17555	2014-12-06T16:40:37	56997.695	55 247	0.945	2.7 ± 0.3	$+167.4 \pm 0.3$
17561	2014-12-20T17:22:40	57011.724	54 567	0.945	2.5 ± 0.2	$+181.5 \pm 0.3$
17562	2014-12-25T15:11:01	57016.633	42 031	0.946	2.2 ± 0.3	$+186.3 \pm 0.3$
16444	2014-12-27T22:58:58	57018.958	41 440	0.942	2.7 ± 0.3	$+188.6 \pm 0.3$
16448	2015-02-14T11:54:08	57067.496	34 599	0.943	2.5 ± 0.3	$+237.1 \pm 0.2$
17602	2015-02-19T13:57:46	57072.582	51 705	0.944	2.4 ± 0.2	$+242.3 \pm 0.3$
16447	2015-03-26T05:26:59	57107.227	26 868	0.944	1.9 ± 0.3	$+276.8 \pm 0.2$
16199	2015-03-27T20:27:05	57108.852	39 461	0.943	2.2 ± 0.3	$+278.5 \pm 0.2$
17640	2015-03-31T13:14:43	57112.552	26 318	0.941	2.3 ± 0.4	$+282.1 \pm 0.2$
17641	2015-04-04T19:45:40	57116.823	24 638	0.939	2.2 ± 0.4	$+286.4 \pm 0.2$

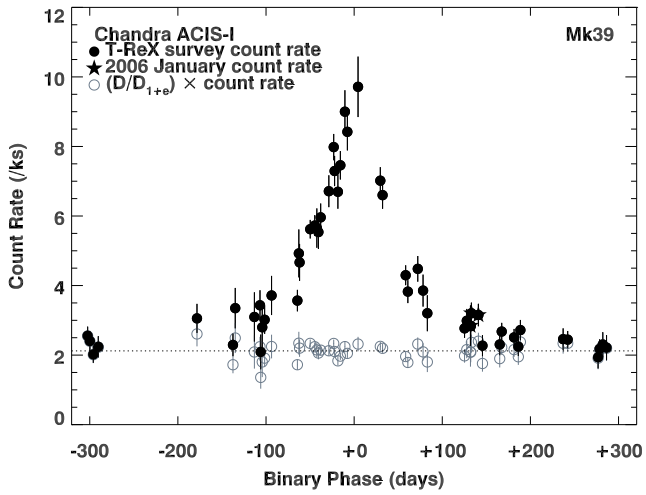

Figure A1. The X-ray orbit of Mk 39 with $P = 641.1$ d and $T_0 = 56830.6$ MJD with observed T-ReX count rates in solid black and the same values adjusted for the implied inverse binary separation shown in open grey.

This paper has been typeset from a TEX/LATEX file prepared by the author.